arXiv:1611.03455v1 [cond-mat.str-el] 10 Nov 2016

Doping driven metal-insulator transitions and charge orderings in the extended Hubbard model

K. J. Kapcia,[1,*] S. Robaszkiewicz,[2] M. Capone,[3] and A. Amaricci[4]

[1] *Institute of Physics, Polish Academy of Sciences, Aleja Lotników 32/46, PL-02668 Warszawa, Poland*
[2] *Faculty of Physics, Adam Mickiewicz University in Poznań, ul. Umultowska 85, PL-61614 Poznań, Poland*
[3] *Scuola Internazionale Superiore di Studi Avanzati (SISSA), Via Bonomea 265, I-34136 Trieste, Italy*
[4] *Scuola Internazionale Superiore di Studi Avanzati and Democritos National Simulation Center, Consiglio Nazionale delle Ricerche, Istituto Officina dei Materiali, Via Bonomea 265, I-34136 Trieste, Italy*

(Dated: November 10, 2016)

We perform a thorough study of an extended Hubbard model featuring local and nearest-neighbor Coulomb repulsion. Using dynamical mean-field theory we investigated the zero temperature phase-diagram of this model as a function of the chemical doping. The interplay between local and non-local interaction drives a variety of phase-transitions connecting two distinct charge-ordered insulators, i.e., half-filled and quarter-filled, a charge-ordered metal and a Mott insulating phase. We characterize these transitions and the relative stability of the solutions and we show that the two interactions conspire to stabilize the quarter-filled charge ordered phase.

PACS numbers: 71.30.+h,71.10.Fd,71.27.+a,71.10.-w

I. INTRODUCTION

Strongly correlated materials are characterized by the relevance of the Coulomb interactions which competes with the kinetic energy, leading to a tendency towards localization of the carriers[1,2]. The simplest theoretical description of this competition is obtained from the Hubbard model[3] in terms of conduction band electrons experiencing a *local* screened Coulomb repulsion. Despite its simplicity, the approximate solutions of this model revealed an incredibly rich physics which has been the object of extensive investigations (e.g. Refs. 4–9). This model is also the starting point to take into account other important effects by including additional interactions, e.g. phonon coupling, orbital ordering or longer-range interaction.

A great deal of attention has been devoted to understand the effects of non-local short-range electron-electron repulsion, which favors a spatial charge ordering[10]. The possible existence of inhomogeneous distribution of charges was firstly predicted in two dimensional (2D) electron gas[11], as a result of the tendency to form a Wigner crystal as soon as the energy gain from the electronic localization tendency exceeds that in the kinetic energy for an homogeneous electron distribution. This possibility has been experimentally realized in various semiconductor structures[12–14]. The effective importance of the electronic interaction for the 2D electrons gas, e.g. layers of liquid Helium, has been recently reconciled with the original Wigner crystallization scenario[15–17]. However other, and somehow more conventional, examples of materials in which charge order interplays with Mott physics can be found in narrow-band correlated systems such as transition-metal dichalcogenides[18,19], or other oxides (e.g. manganites, nickelates, cuprates, bismuthates, and cobaltates)[20–24] as well as low-dimensional organic conductors[25–27] and heavy-fermion systems[28,29].

From a theoretical perspective all these evidences motivated a careful analysis of the Extended Hubbard Model (EHM), i.e. a Hubbard model supplemented with *non-local* density-density interaction term. The direct competition of local and non-local interactions in the EHM captures both the effects of strong correlations and the tendency of the system to form inhomogeneous charge distributions. The EHM has been extensively studied in many different regimes, e.g. strong coupling limit, quarter- and half-filling, and by means of different methods[30–32], such as Hartree-Fock mean-field[30,32–35], Monte Carlo simulations[36–38], variational based cluster perturbation theory[39], lattice exact diagonalization[40–43], two particle self-consistent approach[44], density matrix renormalization group[45,46]. as well as dynamical mean-field theory[16,17,47–49] (DMFT) and its extensions[50–55].

A seminal study of the EHM within DMFT has been reported in Ref. 47 in the quarter-filling case (i.e. for a total density $n = 0.5$). Using a combination of numerical tools it was demonstrated the existence, at large values of the non-local interaction, of a charge-ordered phase separated from the Fermi liquid metal at weak coupling. The origin of such symmetry broken state was interpreted in terms of the effect of strong correlation, signalled by the enhancement of the effective mass. For filling smaller than $n = 0.5$ and specific values of the local and non-local interaction the occurrence of phase-separation between the Fermi liquid and the ordered phase has also been addressed in Ref. 48. However, the existence of a genuine Mott driven Wigner insulating state has been demonstrated only later[16] in the quarter-filling regime. The study of the finite temperature phase-diagram revealed the existence of a strongly correlated charge-ordered metal, separating the Wigner-Mott insulator from the Fermi liquid phase[16,17]. The existence of a $T = 0$ charge-ordered metallic state at quarter-filling has been also shown using cluster exten-

sion of DMFT (CDMFT), which takes into account the role of short-ranged spatial correlation[50]. In particular the onset of charge-order was shown to be concomitant with the occurrence of short range anti-ferromagnetism. More recently, the effects of non-local interaction has been studied in two- and three-dimensional cubic lattice using a combination of GW and Extended DMFT (GW+EDMFT) approach[51–53]. This approach enabled a systematic investigation of the screening effect and the role of longer-range interaction, up to the third nearest neighbor[53]. The solution the EHM by means of GW+EDMFT contributed to clarify the phase-diagram of this model at and near the half-filling regime ($n = 1$)[53], associating the interplay between charge-ordering and correlation to changes in the screening modes.

The emergence of charge-order in strongly correlated systems is also largely affected by geometric frustration factor, which in turn plays a relevant role in different systems, e.g. the charge-transfer salts θ-(BEDT-TTF)$_2$X or the dichalcogenide 1T-TaS_2 both characterized by a triangular-lattice geometry. In this context the interaction driven charge-ordered metal at quarter-filling is associated to the emergence of a quantum phase, i.e. pinball liquid. This state is characterized by quasi-localized charges coexisting with more itinerant electrons, which gives rise to strong quasi-particles renormalization with a mechanism analogous to the heavy fermion compounds[49]. In the multi-orbital case[56], which is relevant for transition-metal oxides, the onset of a pinball phase has been associated to the a finite value of the Hund's exchange[57].

Motivated by the experimental findings and the increasing theoretical work to understand the nature of strongly correlated electronic phases in presence of charge ordering, in this paper we investigate the ground state properties of the EHM. We solve the model using DMFT with zero temperature Lanczos-based exact diagonalization algorithm. We present a thorough investigation of the evolution of the phase-diagram as a function of the local and non-local interaction for an arbitrary occupation of the system. We unveil the properties of the different phase-transitions among the multiple phases characterizing the phase-diagram of the system, in a full range of variation of the model parameters. In particular, we address the first- or second-order nature of the transitions separating the charge-ordered states from normal (disordered) phases. We study the behavior of the order parameter and other relevant quantities including the evolution of the spectral functions. By evaluating the grand-canonical potential, we also determine the meta-stability of the solutions across the phase-transitions and unveil the existence of phase-separation in the phase-diagram.

The rest part of this paper is organized as follows. In Sec. II, we introduce the model and the method of solution. We also discuss the solution of the model in two limiting case. In Sec. III we briefly present the half-filling $n = 1$ solution of the model and discuss the evolution of the phase-diagram as a function of the chemical potential for an increasing value of the interactions. In Sec. IV we present a detailed analysis for each of the multiple phase-transitions occurring in the system. Finally in Sec. V we summarize the results of this work and provide some future perspectives.

II. MODEL AND METHOD

We consider the EHM, which describes the effects of the Coulomb repulsion onto conduction band electrons in terms of a local and a nearest-neighbour density-density interaction. The model Hamiltonian reads:

$$\hat{H} = -t \sum_{\langle i,j\rangle,\sigma} \hat{c}^{+}_{i\sigma}\hat{c}_{j\sigma} + U\sum_{i} \hat{n}_{i\uparrow}\hat{n}_{i\downarrow} + \frac{W}{2}\sum_{\langle i,j\rangle} \hat{n}_i\hat{n}_j - \mu\sum_{i}\hat{n}_i \tag{1}$$

where $\langle i,j\rangle$ indicates summation over nearest-neighbor (NN) sites independently. The parameter t is the hopping amplitude, $\hat{c}^{+}_{i\sigma}$ ($\hat{c}_{i\sigma}$) denotes the creation (destruction) operator of an electron of spin $\sigma =\uparrow,\downarrow$ at the site i. The operators $\hat{n}_i = \sum_\sigma \hat{n}_{i\sigma}$, $\hat{n}_{i\sigma} = \hat{c}^{+}_{i\sigma}\hat{c}_{i\sigma}$, denote the occupation number. Finally μ is the chemical potential. The Hamiltonian terms proportional to U and W describe, respectively, the local and the non-local (NN) part of the screened Coulomb interaction. The competition between these two terms enables to capture the interplay of strong correlation with charge-ordering effects.

DMFT solution – We study the solution of the model (1) using DMFT[6]. In order to allow for a long-range charge ordered phase (check-board type) the lattice is divided into two sub-lattices, indexed by $\alpha = A, B$. The local nature of the DMFT approach does not allow to accurately describe non-local interaction terms[51,52]. To overcome this problem we treat the W term at the mean-field level. The corresponding decoupled Hamiltonian reads:

$$\begin{aligned}\hat{H}_{\rm MF} = &-t \sum_{\langle i,j\rangle,\sigma} \hat{c}^{+}_{i\sigma}\hat{c}_{j\sigma} \\ &+ \sum_{\alpha=A,B}\sum_{i\in\alpha} \left[U\hat{n}_{i\uparrow}\hat{n}_{i\downarrow} - (\mu - Wn_{\bar{\alpha}})\,\hat{n}_i\right] + C,\end{aligned} \tag{2}$$

with $C = -\frac{1}{2}W(n^2 - \Delta^2)$ an inessential constant term.

To fix ideas and to further simplify the treatment we shall consider the case of the Bethe lattice, i.e. a Cayley tree with coordination number $z \to +\infty$. The DMFT approximation becomes exact in this limit, provided t and W are rescaled, respectively, as $t \to t/\sqrt{z}$ and $W \to W/z$[58]. In the same limit the decoupling of the W term is exact, since only Hartree diagram survives[59]. The Bethe Lattice is characterized by a semi-elliptic density of states (per spin):

$$\rho_0(\epsilon) = \frac{2}{\pi D^2}\sqrt{1 - (\epsilon/D)^2} \quad \text{for} \quad |\epsilon| < D. \tag{3}$$

Where $D = 2t$ is the half-bandwidth (or typical kinetic energy) $D = 2\sqrt{\int_{-\infty}^{+\infty} \epsilon^2\rho_0(\epsilon)d\epsilon}$. In the following we set $D = 1$ as the energy unit.

Within DMFT the quantum many-body lattice problem (2) is mapped onto two distinct effective impurity problems, one per sub-lattice. The effective baths are described in terms of frequency dependent Weiss Fields $\boldsymbol{\mathcal{G}}_0^{-1}(i\omega_n) = \text{Diag}\left[\mathcal{G}_{0A}^{-1}(i\omega_n), \mathcal{G}_{0B}^{-1}(i\omega_n)\right]$, which are self-consistently determined by requiring to the impurity problems to reproduce the local physics of the lattice system. In this framework the self-energy matrix $\boldsymbol{\Sigma}(i\omega_n)$, describing the effects of interaction at the one-particle level, is approximated by its local part. For each sub-lattice the self-energy function is determined by the solution of the corresponding quantum impurity problem. In terms of the matrix self-energy the DMFT self-consistency condition reads:

$$\boldsymbol{\mathcal{G}}^{-1}(i\omega_n) = \boldsymbol{G}_{\text{loc}}^{-1}(i\omega_n) + \boldsymbol{\Sigma}(i\omega_n) \tag{4}$$

where $\boldsymbol{G}_{\text{loc}}$ is the diagonal matrix of the local interacting lattice Green's function. This equation relates the bath properties, expressed by the Weiss Field, to the local physics of the lattice problem. In terms of the lattice density of states the components of the local Green's function are:

$$G_{loc,\alpha}(i\omega_n) = \zeta_{\bar{\alpha}}(i\omega_n) \int \frac{\rho_0(\epsilon)d\epsilon}{\zeta_A(i\omega_n)\zeta_B(i\omega_n) - \epsilon^2}, \tag{5}$$

where $\alpha = A, B$ and $\zeta_\alpha(i\omega_n) = i\omega_n + \mu - W\langle\hat{n}_{\bar{\alpha}}\rangle - \Sigma_\alpha(i\omega_n)$.

In this work we solve the effective quantum impurity problem using the Exact Diagonalization technique at $T = 0$[60,61]. The effective bath is discretized into a finite number N_b of levels. The ground-state of the corresponding Hamiltonian as well as the impurity Green's functions are determined using the Lanczos technique. Throughout this work we use $N_b = 9$. The whole DMFT algorithm proceeds as follow. For a given bath function $\boldsymbol{\mathcal{G}}_0^{-1}$ the effective quantum impurity problems are solved. The resulting self-energy function $\boldsymbol{\Sigma}$ is used to determine the local interacting Green's function $\boldsymbol{G}_{\text{loc}}$ by means of Eq. (5). Finally, using the self-consistency relation Eq. (4), a new updated Weiss Field is obtained. The self-consistent DMFT equations are solved iteratively until the convergence is reached, usually in few tens iterations. A critical slowing down of the convergence can be observed near a phase-transition.

In the following we restrict our attention to the case $U \geq 0$ and $W \geq 0$ and to the *non-magnetic* phases. Furthermore, the model (1) exhibits particle-hole symmetry (for any U and W), so our results for $n \leq 1$ ($\bar{\mu} < 0$) are holds identically also for $n > 1$ ($\bar{\mu} > 0$) (see, e.g. Ref. 34). Finally, we checked that the occurring phases in this work are solutions with the lowest grand canonical potential (per site).

A. Non-interacting limit

For $U = 0$ ($W > 0$) the model (2) is solved using a standard broken-symmetry Hartree-Fock approximation.

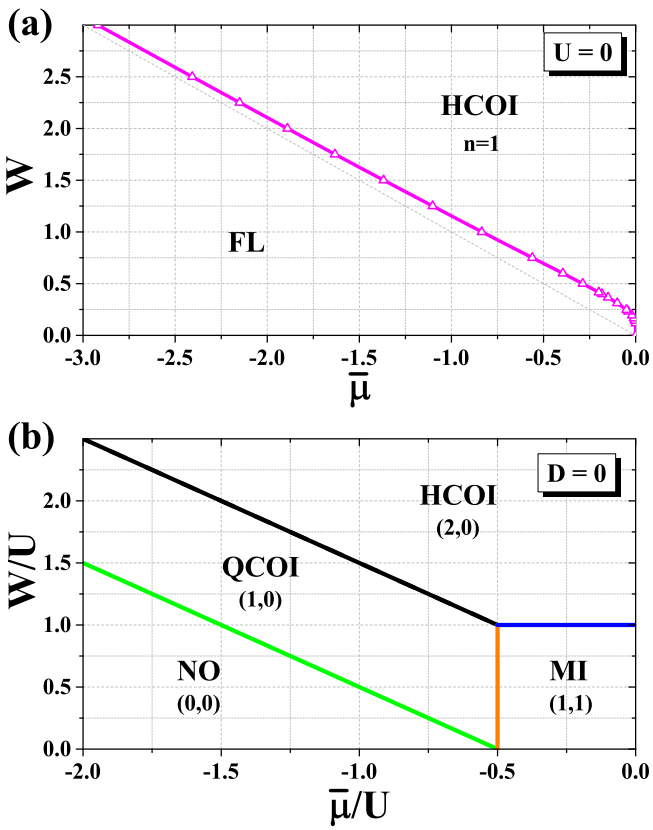

Figure 1. (Color online) (a) Phase diagram for $U = 0$ as a function of W and $\bar{\mu} = \mu - W/2$. The boundary between Fermi Liquid (FL) and half-filled charge-ordered insulator (HCOI) is discontinuous. (b) Phase diagram for $t = 0$ (atomic limit) as a function of the interaction ratio W/U and $\bar{\mu}/U$, $\bar{\mu} = \mu - U/2 - W$. Each phase is labeled by values of (n_A, n_B). All the phases are insulating and all the boundaries are discontinuous.

The mean-field Hamiltonian is diagonalized by means of a Bogoliubov transformation[30,33,62–68]. The resulting self-consistent equations for the total occupation n and the charge polarization $\Delta = \frac{1}{2}(n_A - n_B)$ are:

$$n = \frac{1}{2}\int_{-D}^{D} d\epsilon\rho_0(\epsilon)\left[f(E_1(\epsilon)) + f(E_2(\epsilon))\right], \tag{6}$$

$$\frac{\Delta}{W} = \Delta\int_{-D}^{D} d\epsilon\rho_0(\epsilon)\left[\frac{f(E_1(\epsilon)) - f(E_2(\epsilon))}{2Q(\epsilon)}\right], \tag{7}$$

where $f(x)$ is the Fermi function, $E_{1,2}(\epsilon) = Wn - \mu \mp Q(\epsilon)$ and $Q(\epsilon) = \sqrt{W^2\Delta^2 + \epsilon^2}$[30,33]. The grand canonical potential has the form:

$$\Omega = \bar{C} - \frac{1}{\beta}\sum_{\alpha=1,2}\int d\epsilon\rho_0(\epsilon)\ln\left[1 + \exp\left(-\beta E_\alpha(\epsilon)\right)\right], \tag{8}$$

with $\bar{C} = -\frac{1}{2}W(n^2 - \Delta^2)$.

The non-interacting ground-state phase diagram of model (see Fig. 1(a)) shows the existence of two phases, namely a Fermi liquid metallic state (FL) and a half-filled, i.e. $n = 1$, charge-ordered insulating (HCOI). The

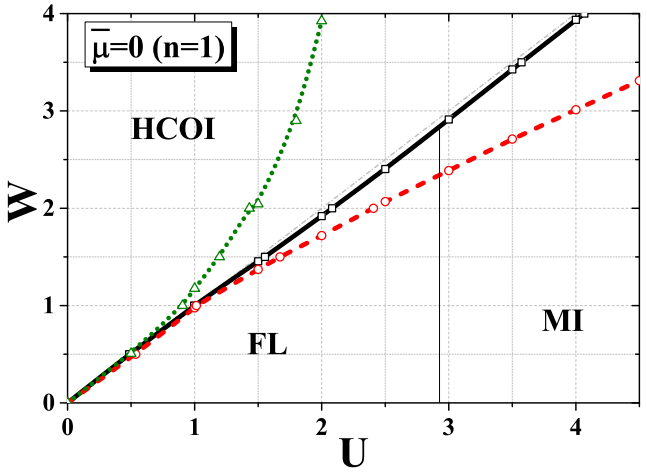

Figure 2. (Color online) Phase diagram in the W-U plane at half-filling, i.e. $n=1$. The solid line (black) at $W/U \simeq 1$ denotes the first-order transition separating the half-filled charge-ordered insulator (HCOI) from the non-ordered phase. The latter includes a Fermi Liquid (FL) metal and a Mott Insulator (MI). The dashed line (red) delimites the region of meta-stability of the HCOI phase. Similarly the dotted line (green) indicates the region of meta-stability for the non-ordered phases.

transition between these two states is of first-order, characterized by a discontinuous change of both the occupation n and the polarization Δ and phase separation for a definite range of n. For $U=0$ any $n\neq 1$ charge-ordered metallic (COM) phase is not stable, i.e. $\partial n/\partial\mu<0$[62–68]. In this limit model (1) is equivalent with the spinless fermion model[62–68].

B. Atomic limit

In the $t=0$ limit the model (2) has been studied in great details (see for example Refs. 69–74 and references therein). Here, we review briefly the rigorous results in the limit $z\to+\infty$ obtained using a variational approach, which treats the on-site U interaction exactly and the intersite W interactions within the mean-field approximation (MFA)[69,72,74]. The ground-state phase diagram for $t=0$ is reported in Fig. 1(b).

The diagram features different COI phases: a quarter-filling one (QCOI) ($n=0.5$) and a HCOI solution. In addition two non-ordered phases are present: a band-insulator for $n=0$ and a Mott insulating phase at $n=1$. Notice that although all transitions are discontinuous, the homogeneous phases occurring for fixed $n\neq 0.5$ or $n\neq 1$ are degenerated with phase separated states. Finite temperature or longer-range intersite interactions however can remove this degeneracy[72,74].

III. PHASE DIAGRAM

We now turn our attention to the combined effect of the local and non-local interaction in the model (2). We first investigated the case of the half-filling, i.e. $\bar{\mu}=0$ and $n=1$. The phase-diagram in the plane U-W is reported in Fig. 2. The figure shows the existence in this regime of three distinct solutions. A HCOI is found for $U\lesssim W$ separated from the normal (non-ordered) solution by a boundary line just below $W/U=1$. The normal solution includes a FL metal at small U and a MI for large enough U. In our approach the FL–MI transition line is roughly independent on W. More accurate calculations, taking into account the non-local interaction beyond the mean-field level, have pointed out that a weak dependence of the Mott transition line on W[52]. In the same diagram of Fig. 2 we also denote the region of meta-stability of the ordered and normal phases enclosed within two spinodal lines. While the HCOI phase extends little into the normal region, we observe that the coexistence region of the non-ordered solution with the HCOI phase rapidly grow with increasing W already for small values of U.

We shall now study the competition of strong correlation and charge-ordering at finite values of the chemical potential $\bar{\mu}$. Our main result is summarized in the phase-diagrams in the plane W-$\bar{\mu}$, reported in Fig. 3. The figure shows the evolution of the diagrams upon increasing the local correlation strength U. For a finite value of U we observe the presence of two additional phases with respect to the non-interacting regime (cf. Fig. 1(a)), namely a charge-ordered metal (COM) and a quarter-filled charge-ordered insulator (QCOI), i.e. $n=0.5$ (Figs. 3(a) and 3(b)). These two phases generically separate the HCOI solution from the Fermi liquid metallic state. A change in the chemical potential $\bar{\mu}$ first destabilizes the HCOI towards the charge ordered metal, occurring at filling $n<1$ and for intermediate values of the non-local interaction W. Further increasing the chemical potential the system reaches the second charge-ordered insulating state, i.e. the QCOI.

The slope of the boundary line of the HCOI is governed by the width of the symmetry related gap, which is linear in W. Upon increasing the strength of the local correlation we observe a substantial modification of the COM and the QCOI regions, with the latter increasing its extension. This is in agreement with the fact that for larger values of U it becomes easier for the depleted system to pin the occupation of a single sub-lattice to a commensurate value, which ultimately favours the formation of a charge-ordered solution. Correspondingly the HCOI region moves towards higher values of W, with the FL-HCOI transition always occurring at $U\simeq W$. Interestingly, the evolution of the boundary line separating the two metallic phases (Fermi liquid and charge-ordered) is not monotonous in U (see Fig. 3). The negative slope of the boundary line in the weak interaction regime (Fig. 3(a)) is progressively transformed into a large positive one at strong coupling (Fig. 3(c)). This

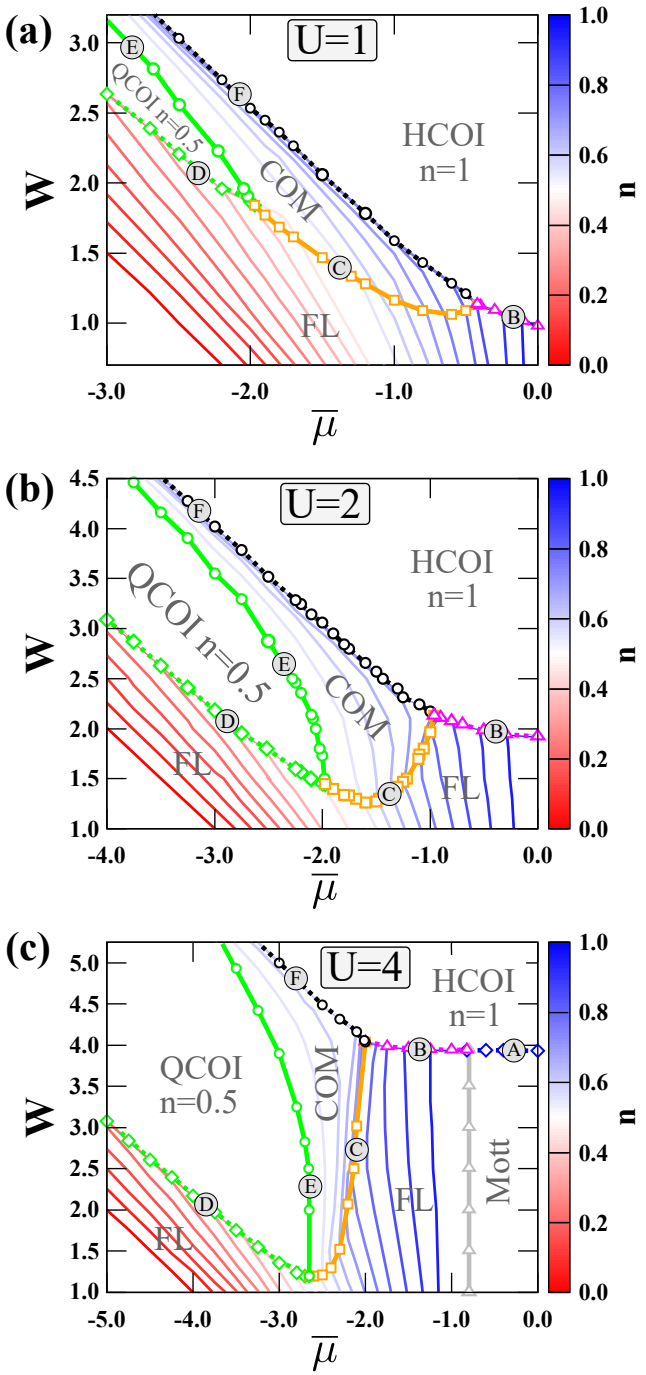

Figure 3. (Color online) The $T = 0$ phase diagrams in the W-$\bar{\mu}$ plane for an increasing value of the local interaction: $U = 1, 2, 4$ (as labeled). The diagrams show the existence of a Fermi Liquid (FL) metallic state at small W, of a charge-ordered metal (COM) for incommensurate occupation as well as different insulating states: a quarter-filled (QCOI), a half-filled charge-ordered insulator (HCOI), and a Mott insulating phase near the $\bar{\mu} = 0$ point. The solid lines (C and E) corresponds to a continuous, i.e. second-order, transitions while the dotted lines (A, B, D and F) indicate the first-order character of the phase-transitions. The letters associated to each boundary line correspond to the paragraphs in Sec. IV. The lines within each diagram are iso-density lines, colored according to the value of the total density n in the right column.

change follows directly the evolution of the total occupation behavior as outlined by the iso-density lines in the diagrams of Fig. 3. By increasing the strength of the local interaction U, the occupation near the FL-COM boundary line becomes nearly independent on W. This behavior is associated to the more localized nature of the metallic state (at small doping) near the Mott insulating phase, occurring for $U \gtrsim 2.92$ near the $\bar{\mu} = 0$ point (see Fig. 3(c)).

IV. PHASE TRANSITIONS

In this section we discuss the properties of the transitions among the different phases of the system. To this end, we shall introduce other distinctive quantities, beside the afore mentioned charge polarization Δ, e.g. the spectral densities at the Fermi level, $\rho_\alpha(0) = -\frac{1}{\pi}\Im G_{\mathrm{loc},\alpha}(\omega = 0)$, and the renormalization constants $Z_\alpha = \left(1 - \frac{\partial \Sigma_\alpha(\omega)}{\partial \omega}_{|_{\omega=0}}\right)^{-1}$ $(\alpha = A, B)$.

A. The MI-HCOI transition

To start with we discuss the transition between the Mott insulator and the HCOI (see Fig. 3(c)). This transition occurs between two phases at half-filling ($n = 1$) and for a large enough value of U in order to guarantee the existence of the Mott insulator. The behavior of the charge polarization Δ as a function of the non-local interaction strength W is reported in Fig. 4(a). The evolution of the order parameter exhibits a discontinuity at the transition point, indicating its first-order nature as expected for a symmetry related transition between two insulating states of different origin. Accordingly, the transition shows a remarkable hysteresis of Δ, associated with the existence of metastable phases on the both sides of the transition (see Fig. 4(a)). The metastable Mott insulating region extends to large values of W even beyond the limit of the figure.

In panels (b)-(c) of Fig. 4 we compare the spectral densities $\rho_\alpha(\omega) = -\frac{1}{\pi}\Im G_{\mathrm{loc},\alpha}(\omega)$ $(\alpha = A, B)$ in the two phases. In the Mott region the spectral functions are characterized by the two contributions at high energy, separated by a gap of the order of U hallmark of the Mott nature of the solution. The asymmetry of the spectrum is associated with the finite value of the non-local term W.

In the HCOI region (see Fig. 4(c)) the spectral density is characterized by a band gap, separating the completely filled sub-lattice A ($n_A \approx 2$) from that of the empty sub-lattice B ($n_B \approx 0$). The gap is related to charge-order phenomenon and has a width of $\simeq 2(W - U/2)\Delta$. Because of its mean-field nature with respect to symmetry breaking transition, the DMFT description of charge-ordered state closely reminds the mean-field solution of the problem[62].

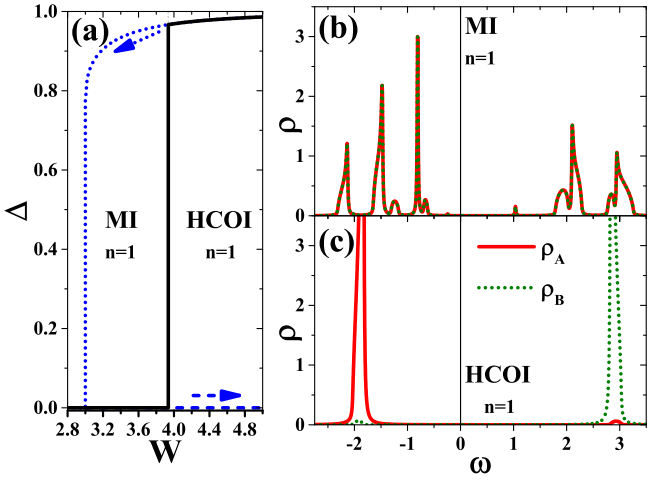

Figure 4. (Color online) The behavior of quantities in the neighborhood of the MI-HCOI boundary. (a) Δ as a function of W for $U=4$ and $\bar{\mu}=-0.5$. The solid, dashed, and dotted lines corresponds to stable, metastable MI, and metastable HCOI solutions, respectively. (b) spectral densities for $W=3.6$ (MI, $n=1$). (c) spectral densities for $W=4.4$ (HCOI, $n=1$). Solid and dotted lines corresponds to different sub-lattices (on (b) and (c) panels). The Fermi level is at $\omega=0$.

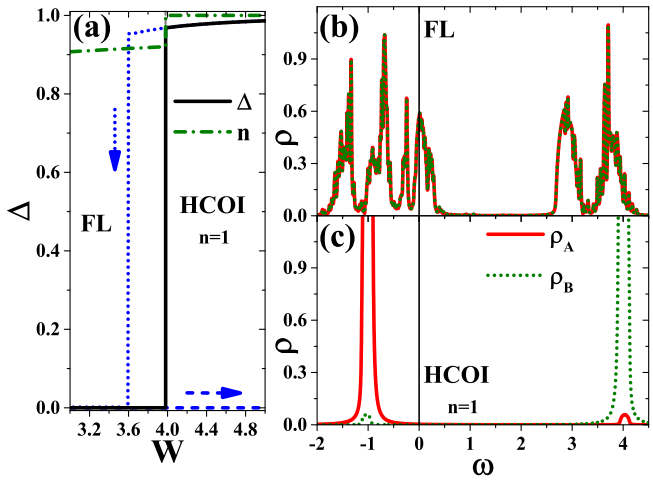

Figure 5. (Color online) The behavior of quantities in the neighborhood of the FL-HCOI boundary. (a) Δ (solid line) and n (dashed-dotted line) as a function of W for $U=4$ and $\bar{\mu}=-1.5$. The dashed and dotted lines corresponds to metastable FL and metastable HCOI solutions, respectively. (b) spectral densities for $W/D=3.6$ (FL). (c) spectral densities for $W/D=4.4$ (HCOI, $n=1$). Solid and dotted lines corresponds to different sub-lattices (on (b) and (c) panels). The Fermi level is at $\omega=0$.

B. The FL-HCOI transition

At finite doping the system admits a transition between the Fermi liquid metal and the HCOI solution. Differently from the previous case this transition occurs between states at different fillings. The behavior of the order parameter Δ and the occupation n across the transition boundary are reported in Fig. 5(a). Both quantities exhibit an abrupt change at the transition. In particular, n evolves discontinuously from $n=1$, in the ordered phase, to $n\approx 0.92<1$ in the normal metallic region. The first-order character of the FL-HCOI transition is further underlined by the hysteresis of Δ. Analogously to the Mott phase, the region of metastability of the FL phase extends to large values of W (beyond the range of the figure).

The spectral functions of the two solutions for the $U=4$ case are reported in Fig. 5(b)-(c). In the FL phase the spectral densities, identical for both sub-lattices $\rho_A(\omega)=\rho_B(\omega)$, have a finite weight at the Fermi level ($\omega=0$) obtained by small doping ($\bar{\mu}=-1.5$) the Mott insulating solution. The quasi-particle resonance at the Fermi level flanks the lower Hubbard band which in turn is separated by a gap of order U from the upper one. In the panel (c) we show the spectral densities for the HCOI phase. The rigid shift with respect to Fig. 4(c) is due the different value of the chemical potential. However the properties of this phase remains unchanged.

C. The FL-COM transition

Similarly, the FL metal can be destabilized towards a COM phase by either increasing the non-local interaction W or the doping value. The symmetry breaking transition relating these two phase at incommensurate filling is continuous, i.e. of second order. Further insight in the continuous character of the transition can be inferred from the behavior of the iso-density lines across the boundary line, see Fig. 3. Approaching the transition from both phases, the density evolves smoothly enabling for the continuous formation/destruction of the charge-polarization. The behavior of the densities $n_{A,B}$ and of the order parameter Δ as a function of W for $U=2$ is reported in Fig. 6(a). Crossing the transition line (see the phase-diagram in Fig. 3) by decreasing W from the COM solution, the order parameter Δ gets continuously reduced to zero. In proximity of the critical point $W=W_c$ the order parameter exhibits the characteristic square-root behavior $\Delta=(W-W_c)^{1/2}$ (see Fig. 6(a)) as expected from a mean-field description of the phase-transition.

In the charge-ordered phase the unbalanced occupations among the two sub-lattices give rise to different degrees of correlation. We quantify this by showing the behavior of the renormalization constants $Z_{A,B}$ across the phase-transition in Fig. 6(b). In particular, the sub-lattice A becomes nearly half-filled ($n_A\simeq 1$) while the other B gets slightly depleted. Correspondingly $Z_A<Z_B$, i.e. the metallic state at A becomes significantly more correlated than the other, less occupied,

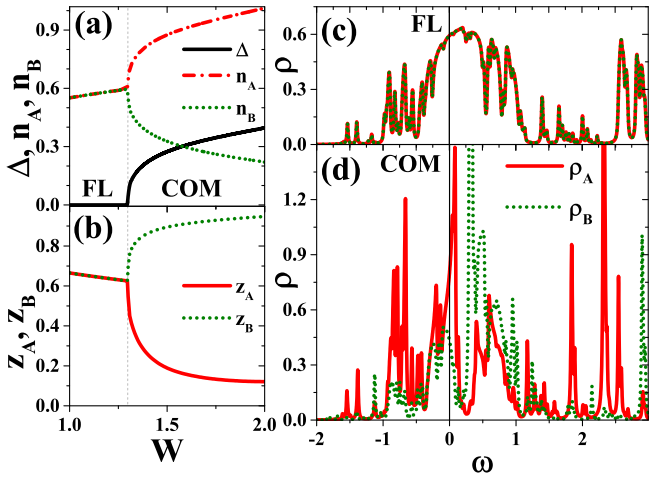

Figure 6. (Color online) The behavior of quantities in the neighborhood of the FL-COM boundary. (a) Δ (solid line), n_A (dashed-dotted line), and n_B (dotted line) as a function of W for $U/D = 2.0$ and $\bar{\mu}/D = -1.5$. (b) z_A (solid line) and z_B (dotted line) as a function of W for the same values of the other parameters. (c) spectral densities for $W = 1.25$ (FL) . (d) spectral densities for $W = 1.35$ (COM). Solid and dotted lines corresponds to different sublattices (on (c) and (d) panels). The Fermi level is at $\omega = 0$.

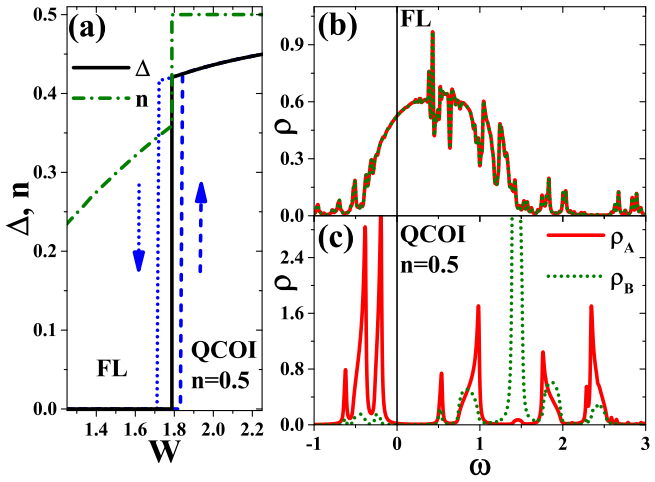

Figure 7. (Color online) The behavior of quantities in the neighborhood of the FL-QCOI boundary. (a) Δ (solid line) and n (dashed-dotted line) as a function of W for $U = 2.0$ and $\bar{\mu} = -2.5$. The dashed and dotted lines corresponds to metastable FL and metastable QCOI solutions, respectively. (b) spectral densities for $W = 1.70$ (FL). (c) spectral densities for $W = 1.85$ (QCOI, $n = 0.5$). Solid and dotted lines corresponds to different sub-lattices (on (b) and (c) panels). The Fermi level is at $\omega = 0$.

sub-lattice.

The different nature of the metallic states at the two phases is also evident from the corresponding spectral functions, reported in Fig. 6(c)-(d). A large featureless spectral weight, reminiscent of the non-interacting (semi-elliptic) distribution, characterizes both sub-lattices in the FL phase. The effect of the large correlation U manifests itself in the contribution at high-energy (Fig. 6(c)). In the charge-order phase the two spectral functions show the formation of a tiny gap slightly away from the Fermi level ($\omega = 0$), as result of the incommensurate filling and to the metallic character of the solution. In this regime the two sub-lattices distributions are nearly specular one with respect to another, with a relative shift of about $2W\Delta$. The strongly correlated nature of the sub-lattice A solution is further underlined by the narrow resonance at the Fermi level characterizing the spectral function at low energy (see Fig. 6(d)). Likewise, precursors of the Hubbard bands are visible in the higher energy region.

D. The FL-QCOI transition

For even larger values of the chemical potential $\bar{\mu}$, i.e. doping, the effect of non-local interaction W is to transform the Fermi liquid metal directly into a QCOI. The transition occurs through the pinning of the occupation to a commensurate value for one sub-lattice with the concomitant opening of a charge-order gap, while the other sub-lattice gets nearly empty. The discontinuous nature of the transition can be further appreciated by looking at the evolution of the iso-density lines near the boundary line. As reported in Fig. 3, near the transition the FL metal has a small occupation while the QCOI is pinned to $n = 0.5$. This prevents the continuous transformation of one state into the other and the only way to connect the two phases is through a first-order jump.

The behavior of the density n and of the order parameter Δ as a function of W across the transition is reported in Fig. 7(a). The occupation n undergoes a jump to $n = 0.5$ for a critical value of the non-local interaction $W = W_c$. At the critical point the charge-polarization Δ suddenly acquires a finite value. The figure also shows the hysteresis cycle of the order-parameter, demonstrating the first-order nature of this transition.

In the panels (b)-(c) of the figure we report the evolution of the spectral functions across the phase-transition. In the FL phase (see Fig. 7(b)), the distribution is characterized by a large featureless spectrum. In this low-density regime and for small W the effects of the local correlation are rather weak. Entering the QCOI region both spectral functions exhibit a gap of the order of $\mathrm{Max}\{2W\Delta, U\}$ at the Fermi level, associated with the charge-order and Mott localization occurring in the system. The spectral weight of the sub-lattice B is located above the Fermi level, corresponding to an almost depleted regime, while the other sub-lattice is nearly half-filled due to intersite repulsion W.

The interplay between both U and W interaction has a strong impact on this phase and, as discussed in Sec. III and Ref. 17, they both contribute to stabilize the QCOI phase. Thus, the occurrence of the QCOI phase is associated with the conventional Mott scenario for the lo-

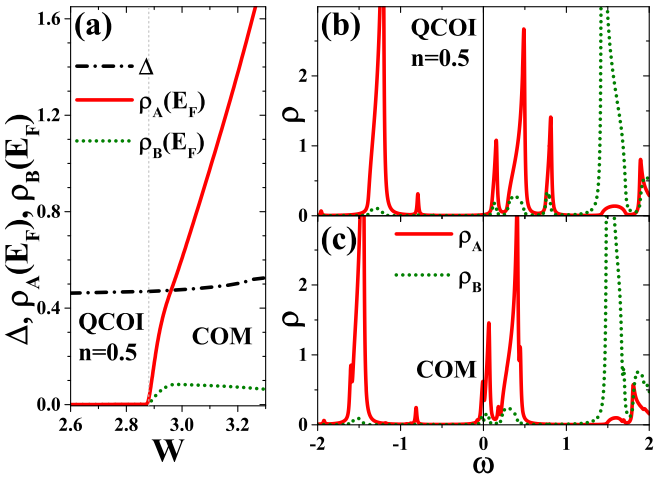

Figure 8. (Color online) The behavior of quantities in the neighborhood of the QCOI–COM boundary. (a) Δ (dashed-dotted line), $\rho_A(E_F)$ (solid line), and $\rho_B(E_F)$ (dotted line) as a function of W for $U=2.0$ and $\bar{\mu}=-2.5$. (b) spectral densities for $W=2.75$ (QCOI, $n=0.5$). (c) spectral densities for $W=3.00$ (COM). Solid and dotted lines corresponds to different sublattices (on (b) and (c) panels). The Fermi level is at $\omega=0$.

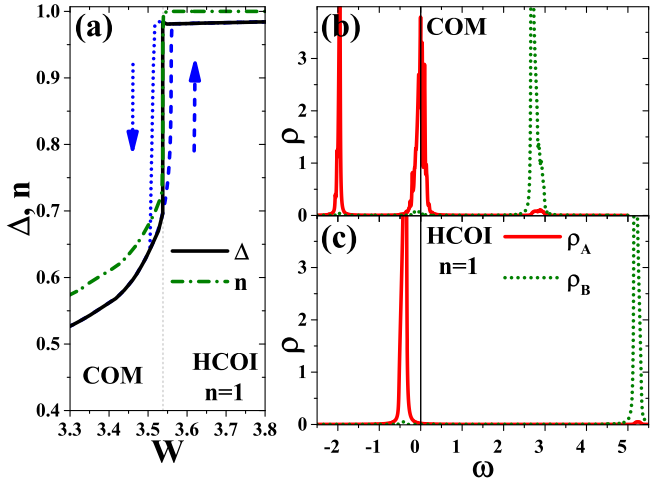

Figure 9. (Color online) The behavior of quantities in the neighborhood of the COM–HCOI boundary. (a) Δ (solid line) and n (dashed-dotted line) as a function of W for $U=2.0$, $\bar{\mu}=-2.5$. The dashed and dotted lines corresponds to metastable COM and metastable HCOI solutions, respectively. (b) spectral densities for $W=3.5$ (COM). (c) spectral densities for $W=3.8$ (HCOI, $n=1$). Solid and dotted lines corresponds to different sub-lattices (on (b) and (c) panels). $\omega=0$ corresponds to the Fermi level.

calization of the electrons in nearly half-filled sub-lattice A, whereas almost empty sub-lattice B is rather band insulator[17].

E. The QCOI-COM transition

The charge-ordered insulating phase at quarter filling can be destabilized by either reducing the doping (i.e. reduce the chemical potential) or increasing W. The resulting insulator to metal transition however occurs without destroying the long range charge order. In Fig. 8(a) we demonstrate this by tuning the non-local interaction W, driving the QCOI into a COM state. In this figure we show that charge polarization Δ remains finite across the transition. We characterize the metallization process through the behavior of the spectral weights at the Fermi level $\rho_{A,B}(E_F\equiv 0)$ across the transition. These quantities show a continuous evolution, corresponding to a second-order phase-transition. In particular, the sub-lattice A which is near the half-filling occupation, rapidly gain a substantial amount of spectral weight at Fermi level developing continuously into a strongly correlated metal, i.e. $Z_A\simeq 0$ (not shown in the figure) in agreement with the Wigner-Mott transition scenario for the electrons at the sub-lattice A[16,17].

The spectral distributions across the transition are reported in Fig. 8(b)-(c). The two cases are characterized by the presence of a large charge-order gap. Within our solution, increasing of the interaction term W cause a small change of the chemical potential, which is sufficient to destabilize the charge-order insulator into a metallic state. However, in a presence of sufficiently strong local and non-local correlation a small doping is not enough to suppress completely the long range ordering, leading to the formation of the COM.

F. The COM-HCOI transition

We finally discuss the properties of the transition from the COM state to the HCOI phase. In Fig. 9(a) we report the behavior as a function of the interaction W of both the total density n and the charge-polarization Δ across the transition line. Differently from the COM-QCOI case discussed previously, the transition from the charge-ordered metallic state to the HCOI has a first-order character. As reported in the figure at the critical point the total density jumps to the $n=1$ value. Correspondingly, the order parameter discontinuously reaches its maximum value. The hysteresis of this quantity is also reported in the figure.

The spectral densities across the transition are shown in Fig. 9(b)-(c). The evolution of the spectra reveals that the metal-insulator transition is driven by a shift of the spectral weight below the Fermi level, i.e. the interaction W drives a shift in the chemical potential increasing the total occupation and a concomitant transfer of the spectral weight. In this regime the large value of W maintains the long range charge order. The HCOI spectrum displays the distinctive features already discussed in the previous sections.

V. CONCLUSIONS

In this work we studied the competition between local and non-local electronic interaction within the paradigmatic extended Hubbard model. We solved the model non-perturbatively using dynamical mean-field theory, with a Lanczos Exact Diagonalization technique. In particular we thoroughly investigated the interplay of charge-ordering and Mott physics as a function of the chemical potential which in turn controls the particle density. We determined the zero temperature phase-diagram as a function of the non-local interaction W and chemical potential $\bar{\mu}$. For any value of local correlation U we reported the existence of both an insulating charge ordered solution at quarter filling and a incommensurate charge ordered metal. These two phases, which have no counterpart in the non-interacting regime, get stabilized by the interplay of local and longer range interaction. The evolution of the phase-diagram as a function of U has shown the increasing stability of the quarter-filled charge-ordered solution.

We studied in details the nature and the properties of the different phase-transitions occurring among the multiple phases of the system. In particular we unveiled the characteristics of the continuous metal-insulator transition separating the charge-ordered metal and the $n=0.5$ insulator, which extends to the incommensurate case previous results available in the recent literature. Moreover, we showed that the small W Fermi liquid metal is separated from the charge-ordered metallic state by a continuous transition and from the quarter-filled charge ordered insulator by a first-order one. The analysis of the iso-density lines enabled us to associate the difference in the transition character to distinct behavior of the occupation in the two regimes. Thus, for example the incommensurate filling of the charge ordered metal can be continuously connected with the Fermi liquid state through the progressive reduction of the charge polarization. On the contrary in the large doping regime, the severe difference in the occupation between the quarter filled charge-ordered insulator and the almost empty Fermi liquid leaves room only to a first order phase-transition.

Although the simple nature the Extended Hubbard Model cannot be regarded as a realistic or quantitatively accurate representation of the real system, its solution in a controlled non-perturbative framework allows to shed light on the microscopic mechanism behind several experimental observations. Notice also that the immense development of experimental techniques in cold atomic Fermi gases on the optical lattices in the last years has opened new opportunities for research of strongly correlated systems and beyond. The ability to precisely control the interactions via Feshbach resonances[75–77] sets new perspectives for experimental realization and study of many different theoretically well-described system, in particular various non-standard Hubbard models (for review see, e.g., Refs. 78 and 79).

Our study demonstrates how the tendency to charge ordering favors and strengthens the transformation of conduction electrons into localized particles in the presence of long-range charge-order. The analysis of the phase-transitions and the destruction of the charge-order at an arbitrary filling can be useful to understand recent experiments on the 2D electron gas from deposed liquid He^3 on a substrate, which corresponds to incommensurate density[80–85].

ACKNOWLEDGMENTS

K.J.K thanks SISSA for the hospitality during his six month research stay in Trieste in 2015. A.A. and M.C. acknowledge financial support from the European Research Council under FPO7 Starting Independent Research Grant n.240524 “SUPERBAD". A.A. also acknowledges support from the European Union, Seventh Framework Programme FP7, under Grant No. 280555 “GO FAST” and under H2020 Framework Programme, ERC Advanced Grant No. 692670 “FIRSTORM” for part of this work. K.J.K was supported by National Science Centre (NCN, Poland) – ETIUDA 1 programme, grant No. DEC-2013/08/T/ST3/00012 in years 2013–2015.

* corresponding author; e-mail:konrad.kapcia@ifpan.edu.pl

[1] P. Fulde, P. Thalmeier, and G. Zwicknagl, in *Solid State Physics Advances in Research and Applications*, Solid State Physics, Vol. 60, edited by H. Ehrenreich and F. Spaepen (Academic Press, 2006) pp. 1–180.
[2] V. Anisimov and Y. Izyumov, *Electronic Structure of Strongly Correlated Materials*, Springer Series in Solid-State Sciences, Vol. 163 (Springer-Verlag Berlin Heidelberg, 2010).
[3] J. Hubbard, Proc. R. Soc. London **276**, 238 (1963).
[4] D. R. Penn, Phys. Rev. **142**, 350 (1966).
[5] J. Spałek, A. Datta, and J. M. Honig, Phys. Rev. Lett. **59**, 728 (1987).
[6] A. Georges, G. Kotliar, W. Krauth, and M. J. Rozenberg, Rev. Mod. Phys. **68**, 13 (1996).
[7] F. Gebhard, *The Mott Metal-Insulator Transition. Models and Method*, Springer Tracts in Modern Physics, Vol. 137 (Springer-Verlag Berlin Heidelberg, 1997).
[8] A. Montorsi, ed., *The Hubbard Model. A Collection of Reprints* (World Scientific, 1992).
[9] J. Vučičević, D. Tanasković, M. J. Rozenberg, and V. Dobrosavljević, Phys. Rev. Lett. **114**, 246402 (2015).
[10] J. Sólyom, EPJ Web of Conferences **78**, 01009 (2014).
[11] E. Wigner, Phys. Rev. **46**, 1002 (1934).

[12] E. Y. Andrei, G. Deville, D. C. Glattli, F. I. B. Williams, E. Paris, and B. Etienne, Phys. Rev. Lett. **60**, 2765 (1988).
[13] Y. Hanein, U. Meirav, D. Shahar, C. C. Li, D. C. Tsui, and H. Shtrikman, Phys. Rev. Lett. **80**, 1288 (1998).
[14] S. V. Kravchenko and M. P. Sarachik, Rep. Prog. Phys. **67**, 1 (2004).
[15] S. Pankov and V. Dobrosavljević, Phys. Rev. B **77**, 085104 (2008).
[16] A. Camjayi, K. Haule, V. Dobrosavljević, and G. Kotliar, Nat. Phys. **4**, 932 (2008).
[17] A. Amaricci, A. Camjayi, K. Haule, G. Kotliar, D. Tanasković, and V. Dobrosavljević, Phys. Rev. B **82**, 155102 (2010).
[18] E. Morosan, H. W. Zandbergen, B. S. Dennis, J. W. G. Bos, Y. Onose, T. Klimczuk, A. P. Ramirez, N. P. Ong, and R. J. Cava, Nat. Phys. **2**, 544 (2006).
[19] A. M. Novello, B. Hildebrand, A. Scarfato, C. Didiot, G. Monney, A. Ubaldini, H. Berger, D. R. Bowler, P. Aebi, and C. Renner, Phys. Rev. B **92**, 081101(R) (2015).
[20] M. Imada, A. Fujimori, and Y. Tokura, Rev. Mod. Phys. **70**, 1039 (1998).
[21] C. Renner, G. Aeppli, B.-G. Kim, Y.-A. Soh, and S.-W. Cheong, Nature **416**, 518 (2002).
[22] T. Goto and B. Lüthi, Adv. Phys. **52**, 67 (2003).
[23] E. Dagotto, T. Hotta, and A. Moreo, Phys. Rep. **344**, 1 (2001).
[24] E. H. da Silva Neto, R. Comin, F. He, R. Sutarto, Y. Jiang, R. L. Greene, G. A. Sawatzky, and A. Damascelli, Science **347**, 282 (2015).
[25] H. Seo, C. Hotta, and H. Fukuyama, Chem. Rev. **104**, 5005 (2004).
[26] D. Jérome, Chem. Rev. **104**, 5565 (2004).
[27] C. Bourbonnais and D. Jérome, "Interacting electrons in quasi-one-dimensional organic superconductors," in *The Physics of Organic Superconductors and Conductors*, edited by A. Lebed (Springer Berlin Heidelberg, Berlin, Heidelberg, 2008) pp. 357–412.
[28] A. Ochiai, T. Suzuki, and T. Kasuya, J. Phys. Soc. Jpn. **59**, 4129 (1990).
[29] P. Fulde, B. Schmidt, and P. Thalmeier, EPL (Europhys. Lett.) **31**, 323 (1995).
[30] S. Robaszkiewicz, Acta Phys. Pol. A **45**, 289 (1974).
[31] H. Lin, D. Campbell, and R. Clay, Chin. J. Phys. **38**, 1 (2000).
[32] A. Hoang and P. Thalmeier, J. Phys.: Condens. Matter **14**, 6639 (2002).
[33] S. Robaszkiewicz, Phys. Stat. Sol. B **59**, K63 (1973).
[34] R. Micnas, J. Ranninger, and S. Robaszkiewicz, Rev. Mod. Phys. **62**, 113 (1990).
[35] K. Rościszewski and A. Oleś, J. Phys.: Condens. Matter **15**, 8363 (2003).
[36] J. E. Hirsch, Phys. Rev. Lett. **53**, 2327 (1984).
[37] H. Q. Lin and J. E. Hirsch, Phys. Rev. B **33**, 8155 (1986).
[38] R. T. Clay, A. W. Sandvik, and D. K. Campbell, Phys. Rev. B **59**, 4665 (1999).
[39] M. Aichhorn, H. G. Evertz, W. von der Linden, and M. Potthoff, Phys. Rev. B **70**, 235107 (2004).
[40] K. Penc and F. Mila, Phys. Rev. B **49**, 9670 (1994).
[41] M. Calandra, J. Merino, and R. H. McKenzie, Phys. Rev. B **66**, 195102 (2002).
[42] J. Merino, H. Seo, and M. Ogata, Phys. Rev. B **71**, 125111 (2005).
[43] S. Fratini and J. Merino, Phys. Rev. B **80**, 165110 (2009).
[44] B. Davoudi and A.-M. S. Tremblay, Phys. Rev. B **74**, 035113 (2006).
[45] M. Vojta, R. E. Hetzel, and R. M. Noack, Phys. Rev. B **60**, R8417(R) (1999).
[46] M. Vojta, A. Hübsch, and R. M. Noack, Phys. Rev. B **63**, 045105 (2001).
[47] R. Pietig, R. Bulla, and S. Blawid, Phys. Rev. Lett. **82**, 4046 (1999).
[48] N.-H. Tong, S.-Q. Shen, and R. Bulla, Phys. Rev. B **70**, 085118 (2004).
[49] J. Merino, A. Ralko, and S. Fratini, Phys. Rev. Lett. **111**, 126403 (2013).
[50] J. Merino, Phys. Rev. Lett. **99**, 036404 (2007).
[51] T. Ayral, P. Werner, and S. Biermann, Phys. Rev. Lett **109**, 226401 (2012).
[52] T. Ayral, S. Biermann, and P. Werner, Phys. Rev. B **87**, 125149 (2013).
[53] L. Huang, T. Ayral, S. Biermann, and P. Werner, Phys. Rev. B **90**, 195114 (2014).
[54] H. Hafermann, E. G. C. P. van Loon, M. I. Katsnelson, A. I. Lichtenstein, and O. Parcollet, Phys. Rev. B **90**, 235105 (2014).
[55] E. G. C. P. van Loon, A. I. Lichtenstein, M. I. Katsnelson, O. Parcollet, and H. Hafermann, Phys. Rev. B **90**, 235135 (2014).
[56] C. Février, S. Fratini, and A. Ralko, Phys. Rev. B **91**, 245111 (2015).
[57] A. Ralko, J. Merino, and S. Fratini, Phys. Rev. B **91**, 165139 (2015).
[58] W. Metzner and D. Vollhardt, Phys. Rev. Lett. **62**, 324 (1989).
[59] E. Müller-Hartmann, Z. Phys. B **74**, 507 (1989).
[60] M. Caffarel and W. Krauth, Phys. Rev. Lett. **72**, 1545 (1994).
[61] C. Weber, A. Amaricci, M. Capone, and P. B. Littlewood, Phys. Rev. B **86**, 115136 (2012).
[62] R. Vlaming, G. S. Uhrig, and D. Vollhardt, J. Phys.: Condens. Matter **4**, 7773 (1992).
[63] G. S. Uhrig and R. Vlaming, J. Phys.: Condens. Matter **5**, 2561 (1993).
[64] G. S. Uhrig and R. Vlaming, Phys. Rev. Lett. **71**, 271 (1993).
[65] G. S. Uhrig and R. Vlaming, Annalen der Physik **4**, 78 (1995).
[66] W. R. Czart, S. Robaszkiewicz, and B. Tobijaszewska, Acta Phys. Pol. A **114**, 129 (2008).
[67] W. R. Czart, P. R. Grzybowski, M. Nogala, and S. Robaszkiewicz, Acta Phys. Pol. A **121**, 828 (2012).
[68] W. Czart, P. R. Grzybowski, M. Nogala, and S. Robaszkiewicz, Acta Phys. Pol. A **121**, 1042 (2012).
[69] R. Micnas, S. Robaszkiewicz, and K. A. Chao, Phys. Rev. B **29**, 2784 (1984).
[70] F. Mancini and F. P. Mancini, Phys. Rev. E **77**, 061120 (2008).
[71] G. Ganzenmüller and G. Pawłowski, Phys. Rev. E **78**, 036703 (2008).
[72] K. Kapcia and S. Robaszkiewicz, J. Phys.: Condens. Matter **23**, 105601 (2011).
[73] F. Mancini, E. Plekhanov, and G. Sica, Eur. Phys. J. B **86**, 408 (2013).
[74] K. J. Kapcia and S. Robaszkiewicz, Physica A **461**, 487 (2016).
[75] P. O. Fedichev, Y. Kagan, G. V. Shlyapnikov, and J. T. M. Walraven, Phys. Rev. Lett. **77**, 2913 (1996).

[76] G. B. Partridge, W. Li, R. I. Kamar, Y.-a. Liao, and R. G. Hulet, Science **311**, 503 (2006).
[77] C. H. Schunck, Y. Shin, A. Schirotzek, M. W. Zwierlein, and W. Ketterle, Science **316**, 867 (2007).
[78] I. M. Georgescu, S. Ashhab, and F. Nori, Rev. Mod. Phys. **86**, 153 (2014).
[79] O. Dutta, M. Gajda, P. Hauke, M. Lewenstein, D.-S. Lühmann, B. A. Malomed, T. Sowiński, and J. Zakrzewski, Rep. Prog. Phys. **78**, 066001 (2015).
[80] E. Y. Andrei, ed., *Two-Dimensional Electron Systems on Helium and Other Cryogenic Substrates*, Physics and Chemistry of Materials with Low-Dimensional Structures, Vol. 19 (Springer Netherlands, 1997).
[81] M. Haque, I. Paul, and S. Pankov, Phys. Rev. B **68**, 045427 (2003).
[82] D. Konstantinov and K. Kono, Phys. Rev. Lett. **103**, 266808 (2009).
[83] L. V. Levitin, R. G. Bennett, E. V. Surovtsev, J. M. Parpia, B. Cowan, A. J. Casey, and J. Saunders, Phys. Rev. Lett. **111**, 235304 (2013).
[84] H. Yayama and Y. Yatsuyama, J. Low Temp. Phys. **175**, 401 (2014).
[85] K. Aoyama, J. Phys. Soc. Jpn. **83**, 140502 (2014).